

Phase diagram of an extended Agassi modelJ. E. García-Ramos,^{1,2,3} J. Dukelsky,⁴ P. Pérez-Fernández,^{2,5} and J. M. Arias^{2,6}¹*Departamento de Ciencias Integradas y Centro de Estudios Avanzados en Física, Matemática y Computación, Universidad de Huelva, 21071 Huelva, Spain*²*Instituto Carlos I de Física Teórica y Computacional, Universidad de Granada, Fuentenueva s/n, 18071 Granada, Spain*³*Unidad Asociada de la Universidad de Huelva al IEM (CSIC), Madrid, Spain*⁴*Instituto de Estructura de la Materia, CSIC, Serrano 123, 28006 Madrid, Spain*⁵*Departamento de Física Aplicada III, Escuela Técnica Superior de Ingeniería, Universidad de Sevilla, Sevilla, Spain*⁶*Departamento de Física Atómica, Molecular y Nuclear, Facultad de Física, Universidad de Sevilla, Apartado 1065, 41080 Sevilla, Spain*

(Received 2 March 2018; published 2 May 2018)

Background: The Agassi model [D. Agassi, *Nucl. Phys. A* **116**, 49 (1968)] is an extension of the Lipkin-Meshkov-Glick (LMG) model [H. J. Lipkin, N. Meshkov, and A. J. Glick, *Nucl. Phys.* **62**, 188 (1965)] that incorporates the pairing interaction. It is a schematic model that describes the interplay between particle-hole and pair correlations. It was proposed in the 1960s by D. Agassi as a model to simulate the properties of the quadrupole plus pairing model.

Purpose: The aim of this work is to extend a previous study by Davis and Heiss [*J. Phys. G: Nucl. Phys.* **12**, 805 (1986)] generalizing the Agassi model and analyze in detail the phase diagram of the model as well as the different regions with coexistence of several phases.

Method: We solve the model Hamiltonian through the Hartree-Fock-Bogoliubov (HFB) approximation, introducing two variational parameters that play the role of order parameters. We also compare the HFB calculations with the exact ones.

Results: We obtain the phase diagram of the model and classify the order of the different quantum phase transitions appearing in the diagram. The phase diagram presents broad regions where several phases, up to three, coexist. Moreover, there is also a line and a point where four and five phases are degenerated, respectively.

Conclusions: The phase diagram of the extended Agassi model presents a rich variety of phases. Phase coexistence is present in extended areas of the parameter space. The model could be an important tool for benchmarking novel many-body approximations.

DOI: [10.1103/PhysRevC.97.054303](https://doi.org/10.1103/PhysRevC.97.054303)**I. INTRODUCTION**

Algebraic bosonic and fermionic models with few degrees of freedom, that arose in different areas of physics, served for many years as excellent test beds for many-body approximations appropriate for different areas of interest. They are characterized by a simple Lie group structure [1] and can be solved either analytically, if a dynamical symmetry is realized, or numerically, for very large system sizes. Let us mention as typical examples, the Jaynes-Cummings [2] and Dicke [3] models in quantum optics, the Lipkin-Meshkov-Glick (LMG) model [4], the two-level pairing model [5], and the Elliot SU(3) model [6], together with the more recent interacting boson model [7] in nuclear physics. The tremendous success of these models let them to permeate other areas of physics like quantum chemistry, condensed matter, and cold atom physics.

More recently, the study of quantum phase transitions (QPTs) and critical points in algebraic models has been an intensive field of research (see, e.g., Refs. [8] and [9]). Two of the models that we mentioned above, the LMG model, describing monopole-monopole interactions, and the two-level pairing model were combined by Agassi [10] into a single model with an SO(5) group algebra (see also Ref. [11]). The

Agassi model has been scarcely used in the literature in spite of its great flexibility and its simplicity to be solved for large systems. Although the random-phase approximation (RPA), Hartree-Fock-Bogoliubov (HFB) [10–12], and perturbation theory [13] were applied to this model, modern many-body theories of intensive use in nuclear physics did not profit of the model to assess their applicability and accuracy. As an exception, a recent paper explored the merging of coupled cluster theory and symmetry breaking and restoration [14] with the aim posed in future applications to nuclear physics and quantum chemistry.

The Agassi model has a very rich phase diagram explored in Ref. [12] with a parity broken phase related to the monopole interaction and a superconducting one associated to the pairing interaction. We here extend the Agassi model adding a more general monopole interaction that gives rise to a more complex phase diagram and to several QPTs of different character. We study the model within the mean-field HFB theory and compare with exact diagonalizations in large systems. We also explore the behavior of the appropriate order parameters and derive several critical exponents.

The paper is organized as follows: In Sec. II we present the algebraic structure of the Agassi model and introduce its

extension with a new term in the Hamiltonian. In Sec. III, the HFB approach is applied to obtain the mean-field energy surfaces and to analyze the stability of the two families of energy surfaces of the model. In Sec. IV, the structure of the phase diagram and the nature of the QPTs are established, and, finally, in Sec. V, the summary and conclusions of this work are presented.

II. THE EXTENDED AGASSI MODEL

The model space of the Agassi model consists of two levels, each of them with a degeneracy Ω , with Ω being an even number. The single-particle states will be labeled accordingly to the level, $\sigma = 1$ for the upper level and $\sigma = -1$ for the lower one, and to a magnetic quantum number $m = \pm 1, \pm 2, \dots, \pm \Omega/2$, which labels the states within a given level. Therefore, the model space can be physically interpreted as two subshells that are part of a major shell. Hence, $\Omega = 2j$, with j an integer number. Moreover, σ can be considered as the parity of the level, positive for $\sigma = +1$ and negative for $\sigma = -1$.

The Hamiltonian of the extended Agassi model can be written as

$$H = \varepsilon J^0 - g \sum_{\sigma\sigma'} A_{\sigma}^{\dagger} A_{\sigma'} - \frac{V}{2} [(J^+)^2 + (J^-)^2] - 2h A_0^{\dagger} A_0. \quad (1)$$

Please note that the original Agassi model does not contain the last term in (1), $-2h A_0^{\dagger} A_0$. As we will see, this term introduces new physical effects with respect to the original formulation of the model.

In this work we will redefine the Hamiltonian parameters for convenience, introducing the new parameters χ , Σ , and Λ (see Ref. [12]) which are rescaled accordingly to the size of the shell

$$V = \frac{\varepsilon\chi}{2j-1}, \quad g = \frac{\varepsilon\Sigma}{2j-1}, \quad h = \frac{\varepsilon\Lambda}{2j-1}. \quad (2)$$

We assume the above three parameters as positive because otherwise this will lead to unphysical situations. Thus, our extended Agassi Hamiltonian reads

$$H = \varepsilon \left[J^0 - \frac{\Sigma}{2j-1} \sum_{\sigma\sigma'} A_{\sigma}^{\dagger} A_{\sigma'} - \frac{\chi}{2(2j-1)} [(J^+)^2 + (J^-)^2] - 2 \frac{\Lambda}{2j-1} A_0^{\dagger} A_0 \right]. \quad (3)$$

The operators appearing in the Hamiltonian (3) are defined as

$$\begin{aligned} J^+ &= \sum_{m=-j}^j c_{1,m}^{\dagger} c_{-1,m} = (J^-)^{\dagger}, \\ J^0 &= \frac{1}{2} \sum_{m=-j}^j (c_{1,m}^{\dagger} c_{1,m} - c_{-1,m}^{\dagger} c_{-1,m}), \\ A_1^{\dagger} &= \sum_{m=1}^j c_{1,m}^{\dagger} c_{1,-m}^{\dagger}, \quad A_{-1}^{\dagger} = \sum_{m=1}^j c_{-1,m}^{\dagger} c_{-1,-m}^{\dagger}, \end{aligned} \quad (4)$$

$$A_0^{\dagger} = \sum_{m=1}^j (c_{-1,m}^{\dagger} c_{1,-m}^{\dagger} - c_{-1,-m}^{\dagger} c_{1,m}^{\dagger}), \quad (5)$$

$$A_1 = \sum_{m=1}^j c_{1,-m} c_{1,m}, \quad A_{-1} = \sum_{m=1}^j c_{-1,-m} c_{-1,m},$$

$$A_0 = \sum_{m=1}^j (c_{1,-m} c_{-1,m} - c_{1,m} c_{-1,-m}), \quad (6)$$

$$N_{\sigma} = \sum_{m=-j}^j c_{\sigma,m}^{\dagger} c_{\sigma,m}, \quad N = N_1 + N_{-1}, \quad (7)$$

where $c_{\sigma,m}^{\dagger}$, $c_{\sigma,m}$ are fermion operators that create and annihilate a fermion, respectively, in the single-particle state $|\sigma, m\rangle$. There are 10 independent generators, 3 J 's, 6 A 's, and the particle number, N . Note that N_1 and N_{-1} are linear combination of J^0 and N . These operators are the generators of the $O(5)$ algebra.

Therefore, the Hamiltonian (3) can be diagonalized with a $O(5)$ basis [10,15]. On the other hand, since the Hamiltonian (3) commutes with the parity operator $e^{-i\pi J^0}$, the eigenstates of the system will have either positive or negative parity.

III. THE HARTREE-FOCK-BOGOLIUBOV APPROACH

In this section we perform the mean-field energy surface study of the extended Agassi model. To this end, and closely following Ref. [12], we will use a Hartree-Fock transformation followed by a Bogoliubov one. This approach is well suited for this model in which the Hamiltonian contains both pairing and monopole interactions. As shown in Ref. [12], nontrivial BCS and Hartree-Fock broken symmetry solutions are obtained. The Hartree-Fock transformation can be written as

$$a_{\eta,m}^{\dagger} = \sum_{\sigma} D_{\eta\sigma} c_{\sigma,m}^{\dagger} \quad (8)$$

and the Bogoliubov one as

$$\begin{aligned} \alpha_{\eta,m}^{\dagger} &= u_{\eta} a_{\eta,m}^{\dagger} - \text{sig}(m) v_{\eta} a_{\eta,-m}, \\ \alpha_{\eta,-m}^{\dagger} &= u_{\eta} a_{\eta,-m}^{\dagger} + \text{sig}(m) v_{\eta} a_{\eta,m}, \end{aligned} \quad (9)$$

where $\text{sig}(m)$ stands for the sign of m , $\text{sig}(m) = +1$ for $m > 0$ and $\text{sig}(m) = -1$ for $m < 0$.

Any calculation in the Agassi model requires us to fix the system size, j , and the number of interacting fermions. For simplicity we will fix the ratio between the number of fermions and the system size. In the following, we will consider that the number of fermions is $2j$, i.e., the system is half filled and, therefore, there is a number of j fermion pairs. Under this assumption, the following conditions are fulfilled:

$$u_{-1}^2 = v_1^2, \quad u_1^2 = v_{-1}^2, \quad v_{\eta}^2 + u_{\eta}^2 = 1. \quad (10)$$

Therefore, the normal density matrix [12] can be written as

$$\begin{aligned} \rho_{\sigma m, \sigma' m'} &= \langle c_{\sigma,m}^{\dagger} c_{\sigma',m'} \rangle \\ &= \sum_{\eta\eta'} D_{\sigma,\eta} D_{\sigma',\eta'} \langle a_{\eta,m}^{\dagger} a_{\eta',m'} \rangle = \delta_{m,m'} \rho_{\sigma,\sigma'}, \end{aligned} \quad (11)$$

where $\rho_{\sigma,\sigma'} = \sum_{\eta} D_{\sigma,\eta} D_{\sigma',\eta} v_{\eta}^2$. On the other hand, the abnormal density matrix [12] is

$$\begin{aligned} \kappa_{\sigma m,\sigma' m'} &= \langle c_{\sigma,m}^{\dagger} c_{\sigma',m'}^{\dagger} \rangle = \sum_{\eta\eta'} D_{\sigma,\eta} D_{\sigma',\eta'} \langle a_{\eta,m}^{\dagger} a_{\eta',m'}^{\dagger} \rangle \\ &= \text{sig}(m) \delta_{m,-m'} \kappa_{\sigma,\sigma'}, \end{aligned} \quad (12)$$

where $\kappa_{\sigma,\sigma'} = \sum_{\eta} D_{\sigma,\eta} D_{\sigma',\eta} u_{\eta} v_{\eta}$.

It is possible to write Hartree-Fock and Bogoliubov transformations in terms of only two variational parameters, φ and β , as written below:

$$D_{1,1} = D_{-1,-1} = \cos \frac{\varphi}{2}, \quad D_{-1,1} = -D_{1,-1} = \sin \frac{\varphi}{2} \quad (13)$$

and

$$v_1 = \sin \frac{\beta}{2}, \quad v_{-1} = \cos \frac{\beta}{2}. \quad (14)$$

Therefore, the normal density matrix results,

$$\begin{aligned} \rho_{1,1} &= \cos^2 \frac{\varphi}{2} \sin^2 \frac{\beta}{2} + \sin^2 \frac{\varphi}{2} \cos^2 \frac{\beta}{2} \\ &= \frac{1}{2} (1 - \cos \varphi \cos \beta), \\ \rho_{-1,-1} &= \sin^2 \frac{\varphi}{2} \sin^2 \frac{\beta}{2} + \cos^2 \frac{\varphi}{2} \cos^2 \frac{\beta}{2} \\ &= \frac{1}{2} (1 + \cos \varphi \cos \beta), \\ \rho_{1,-1} &= \rho_{-1,1} = \cos \frac{\varphi}{2} \sin \frac{\varphi}{2} \sin^2 \frac{\beta}{2} - \cos \frac{\varphi}{2} \sin \frac{\varphi}{2} \cos^2 \frac{\beta}{2} \\ &= -\frac{1}{2} \sin \varphi \cos \beta. \end{aligned} \quad (15)$$

One should note that with the parametrization (13) and (14) and conditions (10), two independent phase selections for u_1 and u_{-1} are possible: (i) $u_{-1} = v_1 = \sin \frac{\beta}{2}$ and $u_1 = v_{-1} = \cos \frac{\beta}{2}$ and (ii) $u_{-1} = v_1 = \sin \frac{\beta}{2}$ and $u_1 = -v_{-1} = -\cos \frac{\beta}{2}$. While the normal density (15) does not depend on the phase selection because the coefficients appear squared, the abnormal density matrix does depend on the phase selected. In particular, using the positive sign for both parameters u_1 and u_{-1} , case (i), one gets

$$\kappa_{\sigma,\sigma'} = \delta_{\sigma\sigma'} \frac{1}{2} \sin \beta, \quad (16)$$

while for the alternative phase selection, case (ii) above, the abnormal density matrix is

$$\begin{aligned} \kappa_{1,1} &= \cos^2 \frac{\varphi}{2} \sin \frac{\beta}{2} \cos \frac{\beta}{2} - \sin^2 \frac{\varphi}{2} \sin \frac{\beta}{2} \cos \frac{\beta}{2} \\ &= \frac{1}{2} \cos \varphi \cos \beta, \\ \kappa_{-1,-1} &= \sin^2 \frac{\varphi}{2} \sin \frac{\beta}{2} \cos \frac{\beta}{2} - \cos^2 \frac{\varphi}{2} \sin \frac{\beta}{2} \cos \frac{\beta}{2} \\ &= -\frac{1}{2} \cos \varphi \cos \beta, \\ \kappa_{1,-1} &= \kappa_{-1,1} = \cos \frac{\varphi}{2} \sin \frac{\varphi}{2} \sin \frac{\beta}{2} \cos \frac{\beta}{2} \\ &\quad + \cos \frac{\varphi}{2} \sin \frac{\varphi}{2} \sin \frac{\beta}{2} \cos \frac{\beta}{2} \\ &= \frac{1}{2} \sin \varphi \sin \beta. \end{aligned} \quad (17)$$

TABLE I. Bogoliubov phase selection.

Phase selection	Surface
$u_{-1} = v_1 = \sin \frac{\beta}{2}; \quad u_1 = v_{-1} = \cos \frac{\beta}{2}$	A
$u_{-1} = v_1 = \sin \frac{\beta}{2}; \quad u_1 = -v_{-1} = -\cos \frac{\beta}{2}$	B

Depending on the phase selection, different energy surfaces (A and B) are obtained. This is summarized in Table I. Once the HFB state is defined, with a given phase selection, as a function of the variational parameters, φ and β , the energy surface is obtained as the expectation value of the Hamiltonian (3),

$$E(\varphi, \beta) = \frac{\langle \text{HFB}(\varphi, \beta) | H | \text{HFB}(\varphi, \beta) \rangle}{\langle \text{HFB}(\varphi, \beta) | \text{HFB}(\varphi, \beta) \rangle}. \quad (18)$$

The surface extrema are studied by minimizing $E(\varphi, \beta)$ with respect to the variational parameters and then analyzing their stability through the eigenvalues of the Hessian matrix. This is done in the following two subsections for the two possible phase selections given in Table I.

A. Energy surface A

This energy surface is obtained with the selection of phases as stated in the first row of Table I. It can be written as

$$E_A = -\varepsilon j \cos \varphi \cos \beta - g j^2 \sin^2 \beta - V j^2 \sin^2 \varphi \cos^2 \beta. \quad (19)$$

In order to present the results, it is convenient to rescale the energy functional with the size j of the system. Then the energy functional reads

$$\frac{E_A}{j\varepsilon} = -\cos \varphi \cos \beta - \frac{\Sigma}{2} \sin^2 \beta - \frac{\chi}{2} \sin^2 \varphi \cos^2 \beta, \quad (20)$$

with ε being an overall constant of energy [note that the term -1 in the denominator of Eqs. (2) is not taken into account because a large value of j is assumed]. Although the order parameters are φ and β , it is convenient to define combinations of them which are easier to be calculated with a diagonalization. These effective order parameters are

$$\frac{\langle J^+ \rangle_A}{j} = \frac{\langle J^- \rangle_A}{j} = \sin \varphi \cos \beta, \quad (21)$$

$$\frac{\langle A_1^+ \rangle_A}{j} = \frac{\langle A_{-1}^+ \rangle_A}{j} = \frac{1}{\sqrt{2}} \sin \beta, \quad \frac{\langle A_0^+ \rangle_A}{j} = 0, \quad (22)$$

where the subindex A refers to the energy E_A .

To study the extrema of (20), first we impose the derivatives of the energy surface to be equal to zero,

$$\begin{aligned} \frac{\partial E_A}{j\varepsilon \partial \beta} &= \sin \beta (\cos \varphi - \Sigma \cos \beta + \chi \sin^2 \varphi \cos \beta) = 0, \\ \frac{\partial E_A}{j\varepsilon \partial \varphi} &= \sin \varphi \cos \beta (1 - \chi \cos \varphi \cos \beta) = 0. \end{aligned} \quad (23)$$

Later, to determine the nature of the extrema, i.e., minima, maxima, or saddle points, we calculate the Hessian matrix (vertical and horizontal lines are included for clarity),

$$\begin{pmatrix} \mathcal{H}_{\varphi,\varphi} & \mathcal{H}_{\varphi,\beta} \\ \mathcal{H}_{\beta,\varphi} & \mathcal{H}_{\beta,\beta} \end{pmatrix} = \begin{bmatrix} \cos(\beta) \cos(\varphi) & -\sin(\beta) \sin(\varphi) \\ -\chi \cos^2(\beta) \cos(2\varphi) & +\frac{\chi}{2} \sin(2\beta) \sin(2\varphi) \\ -\sin(\beta) \sin(\varphi) & \cos(\beta) \cos(\varphi) - \Sigma \cos(2\beta) \\ +\frac{\chi}{2} \sin(2\beta) \sin(2\varphi) & +\chi \cos(2\beta) \sin^2(\varphi) \end{bmatrix}. \quad (24)$$

The solution of equations (23), assuming that $\Sigma \neq \chi$, leads to four cases plus a particular case in which $\Sigma = \chi$. These solutions are

(I-A) $\varphi = \beta = 0$ ($E_A/(j\varepsilon) = -1$). Regardless the values of Σ and χ .

The Hessian matrix is

$$\begin{pmatrix} 1 - \chi & 0 \\ 0 & 1 - \Sigma \end{pmatrix} \quad (25)$$

with eigenvalues $1 - \chi$ and $1 - \Sigma$. Therefore,

$\chi < 1$ and $\Sigma < 1$: it generates a minimum.

$\chi > 1$ and $\Sigma > 1$: it generates a maximum.

$\chi > 1$ and $\Sigma < 1$ or $\chi < 1$ and $\Sigma > 1$: it generates a saddle point.

Both order parameters are equal to 0. Consequently, the surface E_A has spherical minima $E_A/j\varepsilon = -1$ when $\chi < 1$ and $\Sigma < 1$ (independently of the Λ value).

(II-A) $|\varphi| = |\beta| = \frac{\pi}{2}$ ($E_A = -\frac{\Sigma}{2}$). The extrema do not depend on the values of Σ and χ . The Hessian matrix is

$$\begin{pmatrix} 0 & -1 \\ -1 & \Sigma - \chi \end{pmatrix} \quad (26)$$

with eigenvalues $\frac{1}{2}(\Sigma - \chi \pm \sqrt{(\Sigma - \chi)^2 + 4})$. It turns out that both eigenvalues are always of different sign. Therefore, this solution will correspond to a saddle point.

(III-A) $\beta = 0$, $\cos \varphi = \frac{1}{\chi}$ ($E_A/(j\varepsilon) = -\frac{\chi^2+1}{2\chi}$). Valid for $\chi > 1$. The Hessian matrix is in this case

$$\begin{pmatrix} \frac{\chi^2-1}{\chi} & 0 \\ 0 & \chi - \Sigma \end{pmatrix} \quad (27)$$

with obvious eigenvalues: $\frac{\chi^2-1}{\chi}$ and $\chi - \Sigma$. Therefore, for

$\chi > \Sigma$: it generates a minimum.

$\chi < \Sigma$: it generates a saddle point.

The effective order parameters are

$$\begin{aligned} \frac{\langle J^+ \rangle_A}{j} &= \frac{\langle J^- \rangle_A}{j} = \frac{\sqrt{\chi^2 - 1}}{\chi}, \\ \frac{\langle A_1^+ \rangle_A}{j} &= \frac{\langle A_{-1}^+ \rangle_A}{j} = \frac{\langle A_0^+ \rangle_A}{j} = 0. \end{aligned} \quad (28)$$

Assuming a small parameter x such that $\chi = 1 + x$, the critical exponent can be shown to be $\epsilon = 1/2$

$$\frac{\langle J^+ \rangle_A}{j} = \frac{\langle J^- \rangle_A}{j} \sim \sqrt{2x}, \quad (29)$$

this points towards the existence of a second-order QPT.

This solution is linked to a nonzero value of the variational parameter φ associated to the Hartree-Fock transformation [Eq. (13)], and because of that we will call this solution the Hartree-Fock (HF) deformed solution. Consequently, the surface E_A has an HF deformed minimum $E_A/j\varepsilon = -\frac{\chi^2+1}{2\chi}$ when $\chi > 1$ and $\chi > \Sigma$ (independently of the Λ value).

(IV-A) $\varphi = 0$, $\cos \beta = \frac{1}{\Sigma}$ ($E_A/(j\varepsilon) = -\frac{\Sigma^2+1}{2\Sigma}$) for $\Sigma > 1$. The Hessian matrix is in this case

$$\begin{pmatrix} \frac{\Sigma-\chi}{\Sigma^2} & 0 \\ 0 & \frac{\Sigma^2-1}{\Sigma} \end{pmatrix} \quad (30)$$

with obvious eigenvalues: $\frac{\Sigma-\chi}{\Sigma^2}$ and $\frac{\Sigma^2-1}{\Sigma}$.

Therefore, for

$\chi < \Sigma$: it generates a minimum.

$\chi > \Sigma$: it generates a saddle point.

Assuming a small parameter x such that $\Sigma = 1 + x$, the critical exponent can be shown to be $\epsilon = 1/2$,

$$\begin{aligned} \frac{\langle J^+ \rangle_A}{j} &= \frac{\langle J^- \rangle_A}{j} = 0, & \frac{\langle A_1^+ \rangle_A}{j} &= \frac{\langle A_{-1}^+ \rangle_A}{j} \\ &= \frac{\sqrt{\Sigma^2 - 1}}{\sqrt{2\Sigma}} \sim \sqrt{x}. \end{aligned} \quad (31)$$

Again, this points towards the existence of a second-order QPT.

This solution corresponds to a nonzero value of the variational parameter β linked to the Bogoliubov transformation [Eq. (14)], and because of that we will call this solution the BCS deformed solution. Consequently, the surface E_A has a BCS deformed minimum $E_A/j\varepsilon = -\frac{\Sigma^2+1}{2\Sigma}$ when $\Sigma > 1$ and $\chi < \Sigma$ (independently of the Λ value).

(V-A) $\cos \beta \cos \varphi = \frac{1}{\chi}$ ($E_A/(j\varepsilon) = -\frac{\chi^2+1}{2\chi}$) for the particular case $\chi = \Sigma$.

Solutions (III) and (IV) are particular cases of this solution for $\chi = \Sigma$. The solution corresponds to a minimum, with one of the eigenvalues of the Hessian matrix being positive, while the other zero, and therefore this solution corresponds to a kind of closed valley. The degeneracy of solutions (III-A), (IV-A), and (V-A) is an indicator of the presence of a first-order QPT.

B. Energy surface B

This energy surface is obtained with the selection of phases as stated in the second row of Table I. It can be written as

$$\begin{aligned} E_B &= -\varepsilon j \cos \varphi \cos \beta - 2h j^2 \sin^2 \beta \sin^2 \varphi \\ &\quad - V j^2 \sin^2 \varphi \cos^2 \beta. \end{aligned} \quad (32)$$

Again, in order to present the results, it is convenient to rescale the energy functional with the size j of the system. Then, the second energy functional reads

$$\frac{E_B}{j\varepsilon} = -\cos\varphi \cos\beta - \Lambda \sin^2\beta \sin^2\varphi - \frac{\chi}{2} \sin^2\varphi \cos^2\beta. \quad (33)$$

[Note that the factor -1 in the denominator of (2) is not taken into account because a large value of j is assumed]. In this case, the effective order parameters are

$$\frac{\langle J^+ \rangle_B}{j} = \frac{\langle J^- \rangle_B}{j} = \sin\varphi \cos\beta, \quad (34)$$

$$\frac{\langle A_1^+ \rangle_B}{j} = \frac{\langle A_{-1}^+ \rangle_B}{j} = 0, \quad \frac{\langle A_0^+ \rangle_B}{j} = \sin\beta \sin\varphi. \quad (35)$$

To study the extrema of (33), first we impose the derivatives of the energy surface to be equal to zero,

$$\frac{\partial E_B}{j\varepsilon \partial \beta} = \sin\beta [\cos\varphi - (2\Lambda - \chi) \cos\beta \sin^2\varphi] = 0,$$

$$\frac{\partial E_B}{j\varepsilon \partial \varphi} = \sin\varphi [\cos\beta - \cos\varphi - (2\Lambda - \chi) \sin^2\beta \cos\varphi] = 0. \quad (36)$$

Later, to determine the nature of the extrema, i.e., minima, maxima, or saddle points, we calculate the Hessian matrix (vertical and horizontal lines are included for clarity),

$$\left(\begin{array}{c|c} \mathcal{H}_{\varphi,\varphi} & \mathcal{H}_{\varphi,\beta} \\ \hline \mathcal{H}_{\beta,\varphi} & \mathcal{H}_{\beta,\beta} \end{array} \right) = \left[\begin{array}{c|c} \cos(\beta) \cos(\varphi) - \chi \cos(2\varphi) & -\sin(\beta) \sin(\varphi) \\ +(\chi - 2\Lambda) \sin^2(\beta) \cos(2\varphi) & +\frac{1}{2}(\chi - 2\Lambda) \sin(2\beta) \sin(2\varphi) \\ \hline -\sin(\beta) \sin(\varphi) & \cos(\beta) \cos(\varphi) \\ +\frac{1}{2}(\chi - 2\Lambda) \sin(2\beta) \sin(2\varphi) & +(\chi - 2\Lambda) \cos(2\beta) \sin^2(\varphi) \end{array} \right]. \quad (37)$$

The solution of the equations (36) leads to different scenarios. These are as follows:

(I-B) $\beta = 0, \varphi = 0$ ($E_B/(j\varepsilon) = -1$), regardless the values of χ and Λ . In this case, the Hessian matrix is diagonal,

$$\left(\begin{array}{c|c} 1 - \chi & 0 \\ \hline 0 & 1 \end{array} \right), \quad (38)$$

with obvious eigenvalues $1 - \chi$ and 1 , therefore:

$\chi < 1$: it generates a minimum.

$\chi > 1$: it generates a saddle point.

Both order parameters are equal to 0. Consequently, the surface E_B has spherical minima $E_B/j\varepsilon = -1$ independently of the χ, Σ , and Λ values.

(II-B) $\beta = 0, \cos\varphi = \frac{1}{\chi}$ ($E_B/(j\varepsilon) = -\frac{\chi^2+1}{2\chi}$) for $\chi > 1$. The Hessian matrix is

$$\left[\begin{array}{c|c} \frac{\chi^2-1}{\chi} & 0 \\ \hline 0 & \chi + 2\Lambda \left(\frac{1}{\chi^2} - 1 \right) \end{array} \right] \quad (39)$$

with obvious eigenvalues $\frac{\chi^2-1}{\chi}$ and $\chi + 2\Lambda \left(\frac{1}{\chi^2} - 1 \right)$. The first eigenvalue is always positive (remember that $\chi > 1$), and, consequently,

$\Lambda > \frac{1}{2} \frac{\chi^3}{\chi^2-1}$: generates a saddle point.

$\Lambda < \frac{1}{2} \frac{\chi^3}{\chi^2-1}$: generates a minimum.

The order parameters will be

$$\frac{\langle J^+ \rangle_B}{j} = \frac{\langle J^- \rangle_B}{j} = \frac{\sqrt{\chi^2-1}}{\chi}, \quad (40)$$

$$\frac{\langle A_1^+ \rangle_B}{j} = \frac{\langle A_{-1}^+ \rangle_B}{j} = 0, \quad \frac{\langle A_0^+ \rangle_B}{j} = 0. \quad (41)$$

Again, assuming a small parameter x such that $\chi = 1 + x$, the critical exponent can be shown to be $\epsilon =$

$1/2$. This points to the existence of a second-order QPT.

$$\frac{\langle J^+ \rangle_B}{j} = \frac{\langle J^- \rangle_B}{j} \sim \sqrt{2x}. \quad (42)$$

This solution is linked to a nonzero value of the variational parameter φ associated to the Hartree-Fock transformation [Eq. (13)]. Consequently, the surface E_B has a HF deformed minimum $E_B/j\varepsilon = -\frac{\chi^2+1}{2\chi}$ when $\chi > 1$ and $\Lambda < \frac{1}{2} \frac{\chi^3}{\chi^2-1}$ (independently of the Σ value).

(III-B) $|\varphi| = |\beta| = \frac{\pi}{2}$ ($E_B/(j\varepsilon) = -\Lambda$).

The Hessian matrix is

$$\left(\begin{array}{c|c} 2\Lambda & -1 \\ \hline -1 & 2\Lambda - \chi \end{array} \right) \quad (43)$$

with eigenvalues $\frac{1}{2}(4\Lambda - \chi \pm \sqrt{\chi^2 + 4})$. Therefore,

$\Lambda > \frac{1}{4}(\chi + \sqrt{4 + \chi^2})$: it generates a minimum.

$\frac{1}{4}(\chi + \sqrt{4 + \chi^2}) > \Lambda > \frac{1}{4}(\chi - \sqrt{4 + \chi^2})$: it generates a saddle point.

$\Lambda < \frac{1}{4}(\chi - \sqrt{4 + \chi^2}) < 0$: it generates a maximum.

The order parameters will be

$$\frac{\langle J^+ \rangle_B}{j} = \frac{\langle J^- \rangle_B}{j} = 0, \quad (44)$$

$$\frac{\langle A_1^+ \rangle_B}{j} = \frac{\langle A_{-1}^+ \rangle_B}{j} = 0, \quad \frac{\langle A_0^+ \rangle_B}{j} = 1. \quad (45)$$

Solutions (III-B) and (II-B) become degenerated for $\Lambda = \frac{1+\chi^2}{2\chi}$.

Solutions (III-B) and (I-B) become degenerated for $\Lambda = 1$.

Solutions (III-B) and (IV-A) become degenerated for $\Lambda = \frac{1+\Sigma^2}{2\Sigma}$.

Therefore, the existence of this solution points towards the presence of a first-order QPT. This solution is linked to nonzero values of both variational parameters (φ, β), one associated to the Hartree-Fock transformation [Eq. (13)] and the other to the Bogoliubov transformation [Eq. (14)], therefore this is a combined HF-BCS deformed solution. Consequently, the surface E_B has a deformed HF-BCS minimum $E_B/j\varepsilon = -\Lambda$ when $\Lambda > \frac{1}{4}(\chi + \sqrt{4 + \chi^2})$ (independently of the Σ value).

(IV-B) The last solutions of Eqs. (36) imply

$$\cos \varphi = \cos \beta \sin^2 \varphi (2\Lambda - \chi), \quad (46)$$

$$\cos \beta = \cos \varphi [1 + (2\Lambda - \chi) \sin^2 \beta], \quad (47)$$

with an energy

$$E_B/(j\varepsilon) = \frac{1 - 2\sqrt{2\Lambda}\sqrt{2\Lambda - \chi}}{2(2\Lambda - \chi)}. \quad (48)$$

It can be proved that the solutions always correspond to a saddle point.

Once analyzed both surfaces, the phase diagram of the model is obtained in the next section taking into account the competition between both surfaces which give rise to different regions, some of them including coexistence of the three phases: spherical (S), HF deformed (HF), and BCS deformed (BCS), besides the combined HF-BCS deformed solution.

IV. PHASE DIAGRAM

Based on the analysis of the previous section, we can derive a phase diagram with five different phases:

- (i) Symmetric or spherical solution, ($\varphi = 0, \beta = 0$). It corresponds to solutions (I-A) and (I-B) (letters A or B indicate the energy surface).
- (ii) HF deformed solution, ($\cos \varphi = \frac{1}{\chi}$ and $\beta = 0$). It corresponds to solutions (III-A) or (II-B).
- (iii) BCS deformed solutions, ($\varphi = 0$ and $\cos \beta = \frac{1}{\Sigma}$). It corresponds to solution (IV-A).
- (iv) Combined HF-BCS deformed solution, ($\varphi = \frac{\pi}{2}, \beta = \frac{\pi}{2}$). It corresponds to solution (III-B).
- (v) Closed valley ($\cos \varphi \cos \beta = 1/\chi$). It corresponds to solution (V-A).

In Fig. 1 we depict the phase diagram of the model. The phase diagram is built considering that two energy surfaces (A and B) coexist and compete but only one (except when they are degenerate) gives the absolute minimum. Concerning E_A , one has to take into account that their minima only depend on χ and Σ but they do not depend on Λ , and while regarding E_B , their minima only depends on χ and Λ but they do not depend on Σ . The region with $\chi < 1, \Sigma < 1$, and $\Lambda < 1$ corresponds to the symmetric phase and it is represented in the diagram with a red sphere. The red vertical surface $\chi = 1$ with $\Lambda \leq 1$ and $\Sigma \leq 1$ is a second-order QPT. This can be shown easily looking at the energy values for $\chi < 1$ which is $E = -1$ and

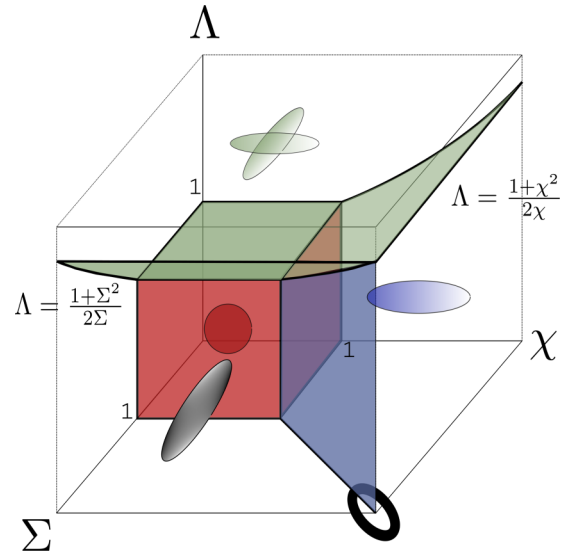


FIG. 1. Phase diagram of the extended Agassi Hamiltonian (3). Red vertical planes correspond to second-order QPT surfaces. The green surface ($\Lambda = 1$ for $\chi < 1$ and $\Sigma < 1$, $\Lambda = \frac{1+\chi^2}{2\chi}$ for $\chi > \Sigma$ and $\Lambda = \frac{1+\Sigma^2}{2\Sigma}$ for $\chi < \Sigma$) and the blue vertical one ($\chi = \Sigma$ and $\Lambda < \frac{1+\Sigma^2}{2\Sigma}$) correspond to first-order critical surfaces. Red sphere, blue oval, black oval, black thick oval, and crossed green ovals stand for the symmetric solution, the HF deformed solution, the BCS deformed solution, the (V-A) solution, and HF-BCS deformed solution, respectively.

for $\chi > 1$ which is $E = -\frac{1+\chi^2}{2\chi}$. These expressions imply a discontinuity in the second-order derivative of the energy at $\chi = 1$. The other red vertical surface $\Sigma = 1$ with $\Lambda \leq 1$ and $\chi \leq 1$, is also a second-order QPT as can be shown by an equivalent argument. The area at the right bottom corresponds to the HF deformed shape and it is depicted with a blue prolate shape oriented in the direction of the χ axis. The area at the left bottom corresponds to the BCS deformed shape and it is represented with a black prolate shape oriented in the direction of the Σ axis. The vertical blue plane with $\chi = \Sigma$ corresponds to a first-order QPT since at this particular surface solutions (III-A) and (IV-A) are degenerated. Besides, solution (V-A) exists, it corresponds to a closed valley in the β - φ plane and it is represented with a black thick oval in the figure. Finally, the region above the green surface corresponds to the solution ($\varphi = \frac{\pi}{2}, \beta = \frac{\pi}{2}$), i.e., to the combined HF-BCS deformed solution and it is represented in the diagram with two crossed green ovals. The green surface corresponds to a first-order QPT since all the energies below the green surface are Λ independent while above $E = -\Lambda$.

In Fig. 1 we represent the deepest minimum of the lowest energy surface. However, because of the presence of two competing energy surfaces, E_A and E_B , there are areas where different phases coexist. These regions have not been depicted in Fig. 1 because of the complexity that would generate in the phase the diagram. For E_A the spherical, the HF deformed, and the BCS deformed solutions cannot coexist. However, for E_B different phases can coexist: (i) the spherical and the combined HF-BCS deformed shape and (ii) the combined HF-BCS and

the HF deformed. Moreover, the competition between E_A and E_B produces the coexistence of up to five different minima:

- (i) Spherical ($\varphi = 0, \beta = 0$), HF-BCS deformed minimum ($\varphi = \pi/2, \beta = \pi/2$), and BCS deformed one ($\varphi = 0, \beta = \arccos(1/\Sigma)$).
- (ii) HF-BCS deformed minimum ($\varphi = \pi/2, \beta = \pi/2$), HF deformed minimum in ($\varphi = \arccos(1/\chi), \beta = 0$) and BCS deformed one in ($\varphi = 0, \beta = \arccos(1/\Sigma)$).
- (iii) Closed valley minimum (for $\Sigma = \chi$) and the combined HF-BCS deformed minimum ($\varphi = \pi/2, \beta = \pi/2$).
- (iv) HF-BCS deformed minimum ($\varphi = \pi/2, \beta = \pi/2$), HF deformed minimum in ($\varphi = \arccos(1/\chi), \beta = 0$), BCS deformed minimum and the closed valley minimum along the line $\Lambda = \frac{1+\chi^2}{2\chi}$ with $\chi = \Sigma$. All the minima are degenerated.
- (v) Spherical ($\varphi = 0, \beta = 0$), HF-BCS deformed minimum ($\varphi = \pi/2, \beta = \pi/2$), BCS deformed one ($\varphi = 0, \beta = \arccos(1/\Sigma)$), HF deformed minimum in ($\varphi = \arccos(1/\chi), \beta = 0$), and the closed valley minimum at the point $\chi = \Sigma = \Lambda = 1$. All the minima are degenerated.

In order to have a more clear image of the phase diagram, in Fig. 2 we present two-dimensional plots in which one of the control parameters has been kept constant. In Fig. 2(a) we depict the plane $\chi = 0.75$. Since $\chi < 1$ the spherical (red S) minimum (I-B) always exists. For $\Sigma > 1$ the BCS deformed minimum (black B) also exists (IV-A). For $\Lambda > \frac{1}{4}(\chi + \sqrt{4 + \chi^2})$, which is the spinodal line (full magenta line) of E_B , the HF-BCS combined minimum (green $\pi/2$) appears (III-B). This results in different areas of coexistence as shown in the figure. The largest most left letter gives the deepest minimum, the second most left letter indicates the second deepest minimum, and so on. For instance, in the region $\Sigma > 1$ and $\Lambda > \frac{1+\Sigma^2}{2\Sigma}$ three phases coexist: The HF-BCS deformed is the lowest and then the BCS deformed and the spherical phase is higher in energy. In the region just below, the same three phases coexist but now the lowest is the BCS deformed and then the spherical and the combined HF-BCS deformed solution is higher in energy.

In Fig. 2(b) we present the case $\Sigma = 1.5$. For $\chi < 1$, the spherical phase, (I-B), always is present. For $\chi < \Sigma$, the BCS deformed minimum, (IV-A), exists. For $\Lambda > \frac{1}{4}(\chi + \sqrt{4 + \chi^2})$, which is the spinodal line (lowest full magenta line) of E_B , the HF-BCS combined minimum (green $\pi/2$) appears, (III-B). For $\chi > \Sigma$ the HF solution, (III-A), always exists. In addition, in the region $1 < \chi < \Sigma$ and $\Lambda < \frac{1}{2} \frac{\chi^3}{\chi^2 - 1}$, which is the antispinodal line (upper full magenta line), the HF deformed solution, (II-B), also exists. Again, different coexistence regions appear as marked in the figure following the same criteria as in Fig. 2(a).

In Fig. 2(c) we analyze the vertical plane $\Lambda = 1.1$. We consider this particular case because it corresponds to a range of parameters in which the most complex situation exists. For $\chi < 1$ the spherical minimum, (I-B), always exists. For $\chi < \Sigma$ and $\Sigma > 1$ the BCS deformed solution, (IV-A), exists. For $\chi < \frac{4\Lambda^2 - 1}{2\Lambda}$, rightmost magenta line [which is obtained from the

spinodal line $\Lambda = \frac{1}{4}(\chi + \sqrt{4 + \chi^2})$] the combined HF-BCS deformed solution exists, (III-B). For $\chi > \Sigma$ and $\chi > 1$ the HF deformed solution exists, (III-A). In addition, there exists the HF deformed solution, (II-B), for $\chi > 1$ and $\Sigma > \chi$ and fulfilling the condition related to the antispinodal line, $\Lambda < \frac{1}{2} \frac{\chi^3}{\chi^2 - 1}$. Different coexistence regions appear as marked in the figure following the same criteria as in Fig. 2(a).

In summary, the phase diagram presents four regions where the shapes are S, HF deformed, BCS deformed, and combined HF-BCS deformed, respectively. However, in each region several minima exist, coexisting up to three phases in certain regions. In addition, there is a line, $\chi = \Sigma$ with $\Lambda = \frac{1+\chi^2}{2\chi}$, in which four phases, HF, BCS, HF-BCS, and the closed valley solutions, are degenerated, plus a single point, $\chi = \Sigma = \Lambda = 1$, in which the five solutions (same as before plus the spherical) are degenerated. Such a rich phase diagram does not appear even in the case of more complex systems, such as the proton-neutron interacting boson model [16], the two-fluid Lipkin model [17], or for Hamiltonians with up to two three-body interactions [18].

V. COMPARISON BETWEEN EXACT AND HARTREE-FOCK-BOGOLIUBOV RESULTS

In this section we present several cases where we calculate, by an exact diagonalization of the Hamiltonian, the values of the ground-state energy and of different effective order parameters and compare them with the HFB results.

We define the effective order parameters in terms of the expectation values of the following operators for the ground state, although, in general, they can be used with excited states:

$$OP_{J^2} = \frac{\langle (J^+)^2 \rangle + \langle (J^-)^2 \rangle}{2j^2}, \quad (49)$$

$$OP_{A_0^2} = \frac{\langle A_0^+ A_0 \rangle}{j^2}, \quad (50)$$

$$OP_{A_1^2} = \frac{\langle A_1^+ A_1 \rangle + \langle A_{-1}^+ A_{-1} \rangle}{2j^2}. \quad (51)$$

Note that these quantities differ from Eqs. (21) and (22) or Eqs. (34) and (35) since the expectation values of single operators J^+ , J^- , A_0 , A_1 , and A_{-1} vanish owing to parity conservation in the exact solution. Therefore, Eqs. (49)–(51) should be compared with the square of either Eqs. (21) and (22) or Eqs. (34) and (35).

All the diagonalizations presented in this section are performed for systems with $j = 100$ (100 pairs of fermions), $\varepsilon = 1$, and only positive-parity states are considered. This number of fermion pairs is large enough to guarantee a good agreement between the HFB mean-field values and the exact ones.

First, we consider a trajectory that goes through one of the red vertical surfaces and, therefore, should correspond to cross a second-order QPT. In particular, in Fig. 3 we depict such a situation, for which we fix the parameters $\Sigma = 0.5$ and $\Lambda = 0$, which allows us to vary the value of χ between 0 and 1.5 [see Fig. 3(e) for the schematic trajectory]. All along this trajectory $\beta = 0$, while $\varphi = 0$ for $\chi < 1$ and $\varphi = \arccos \frac{1}{\chi}$ for $\chi > 1$. This means that we explore the transition between spherical

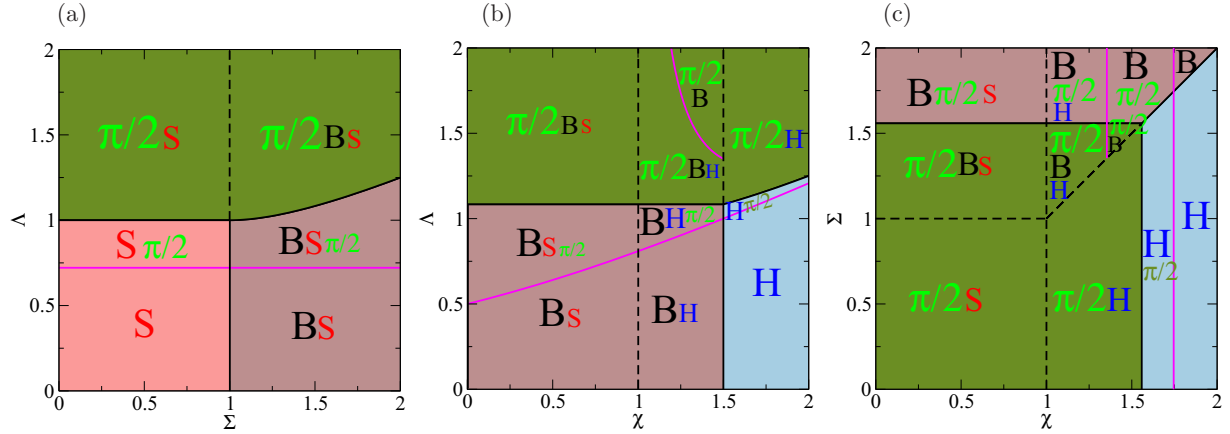


FIG. 2. Phase diagram for selected planes (a) $\chi = 0.75$, (b) $\Sigma = 1.5$, and (c) $\Lambda = 1.1$. Background color represents the shape of the deepest minimum, i.e., light red for the symmetric phase, olive green for combined HF-BCS deformed solution, brown for BCS deformed phase, and light blue for the HF deformed phase. Letters correspond to the existing phases, i.e., red “S” for symmetric phase, green “ $\pi/2$ ” for combined HF-BCS deformed solution, black “B” for the BCS deformed phase, and blue “H” for the HF deformed phase. Larger and leftmost (or upper) letters correspond to deepest minima. Black full lines stand for QPTs, magenta full ones for spinodal-antispinodal lines, and black dashed ones for indicating the change in the ordering of high lying minima.

and HF deformed shapes. In Fig. 3(a), the ground-state energy is shown as a function of χ , suggesting the presence of a second-order QPT around $\chi = 1$. The HFB ground-state energy is -1 for $\chi < 1$ (spherical phase) and $E/(j\varepsilon) = -\frac{\chi^2+1}{2\chi}$ for $\chi > 1$ (HF deformed phase). As stated before, this involves a discontinuity in the second derivative of the energy with respect to χ . In Fig. 3(b), the effective order parameter OP_{J^2} (49) is depicted, and a good agreement between HFB and exact results is obtained. The HFB value is $OP_{J^2} = 0$ for $\chi < 1$, while $OP_{J^2} = 1 - \frac{1}{\chi^2}$ for $\chi > 1$. On the other hand, in spite of the good agreement found with the exact calculations, we can observe a small discrepancy around the critical point $\chi = 1$.

This is due to the finite size of the system. In order to describe properly that region, it is needed to take into account corrections to the size of the system that would improve the results obtained with the HFB approach. In Figs. 3(c) and 3(d) the HFB value of $OP_{A_0^2}$ (50) and $OP_{A_1^2}$ (51) are depicted, respectively, and their analytical values are zero all the way. Note that the vertical scale of these two panels has been multiplied by a factor 100, which can lead the reader to the impression that the agreement is poor, which is not the case because the absolute difference between the exact and analytical results is up to order 10^{-2} . Finally, it is worth noting that this QPT only involves minima of the first energy surface, E_A .

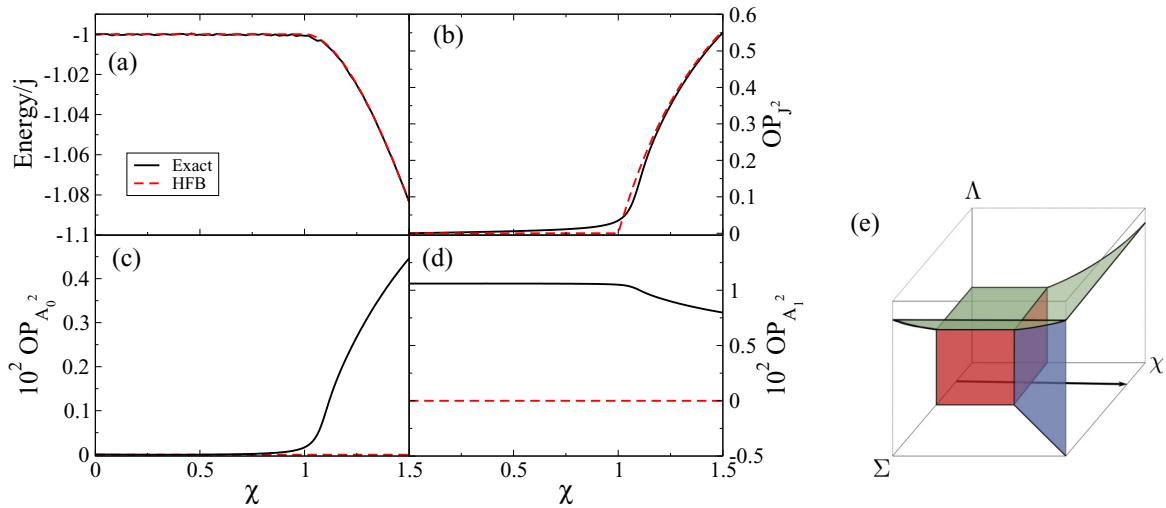


FIG. 3. Comparison of the ground-state energy per fermion pair and order parameter values for HFB and exact results for a system with $j = 100$ and Hamiltonian parameters $\Sigma = 0.5$, $\Lambda = 0$ ($\varepsilon = 1$) as a function of χ . Black full lines correspond to exact results and red dashed ones to HFB ones. Panel (a) corresponds to the ground-state energy, panel (b) to OP_{J^2} , panel (c) to $OP_{A_0^2}$, panel (d) to $OP_{A_1^2}$ order parameters, and panel (e) to the schematic representation of the trajectory in the parameter space. Please note that the scale in panels (c) and (d) is multiplied by 100.

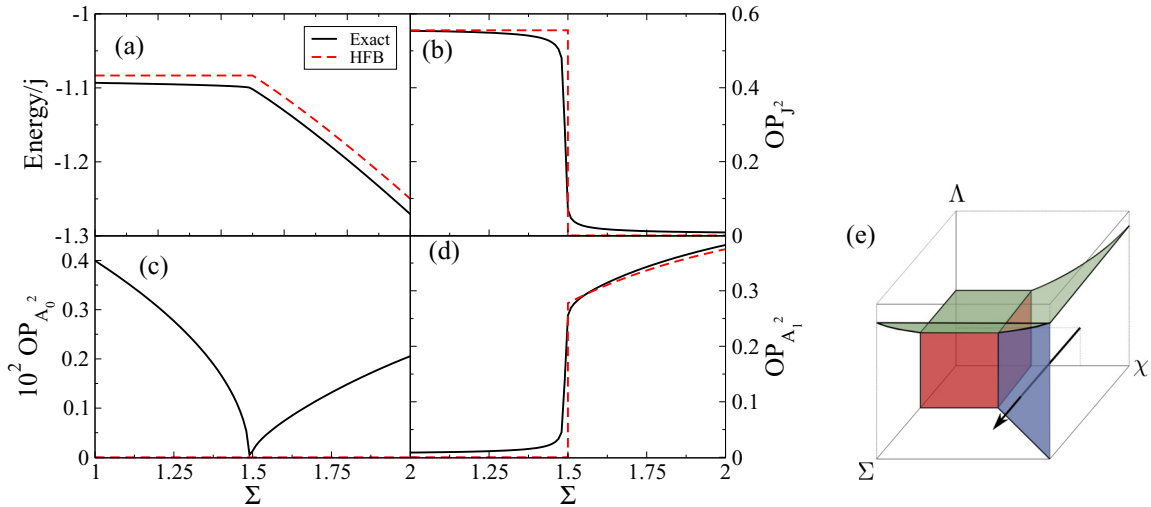


FIG. 4. Same as in Fig. 3 but for $\chi = 1.5$, $\Lambda = 0.5$, as a function of Σ . Please note that the scale in panel (c) is multiplied by 100.

In Fig. 4 we move through the horizontal line $\chi = 1.5$, $\Lambda = 0.5$, as a function of Σ , crossing the $\chi = \Sigma$ vertical plane [see Fig. 4(e)], going from the minimum ($\varphi = \arccos(1/\chi)$, $\beta = 0$) (HF deformed) to ($\varphi = 0$, $\beta = \arccos(1/\Sigma)$) (BCS deformed). As we can see, this QPT transition is of first order, because the HFB energy changes from a constant value $E/(j\varepsilon) = -\frac{1.5^2+1}{2 \cdot 1.5^2}$ for $\Sigma < 1.5$ to $E/(j\varepsilon) = -\frac{\Sigma^2+1}{2\Sigma^2}$ for $\Sigma > 1.5$, with a sudden jump from one minimum to the other, although there is no coexistence. In the case of the HFB value of OP_{J^2} (49) [Fig. 4(b)], the expectation value changes from $OP_{J^2} = 1 - \frac{1}{1.5^2}$ for $\Sigma < 1.5$ to zero for $\Sigma > 1.5$, presenting a discontinuity in the order parameter OP_{J^2} at $\Sigma = 1.5$. On the other hand, in Fig. 4(c) one can see how the HFB value for $OP_{A_0^2}$ (50) is strictly zero for all Σ values, while very small values are obtained in the exact calculation (note that the vertical scale is multiplied by a factor 100). Finally, in Fig. 4(d) the mean-field value for $OP_{A_1^2}$ (51) jumps from zero to $OP_{A_1^2} = 1 - \frac{1}{\Sigma^2}$ at $\Sigma = 1.5$. The exact calculation follows, except

for finite number of particle corrections the same behavior. Note that this QPT only involves minima of the first energy surface, E_A .

Finally, in Fig. 5 we move through a vertical line with $\chi = 1.5$, $\Sigma = 2$, as a function of Λ , crossing the surface $\Lambda = \frac{1+\Sigma^2}{2\Sigma}$ [see Fig. 5(e)], and then passing from ($\varphi = 0, \beta = \arccos(1/\Sigma)$) (deformed BCS) to ($\varphi = \pi/2, \beta = \pi/2$) (combined deformed HF-BCS). The QPT appears at $\Lambda = \frac{1+2^2}{4} = 1.25$. As can be seen in the energy per fermion pair shown in Fig. 5(a), the QPT is, once more, of first order and the HFB energy passes from $E/(j\varepsilon) = -\frac{2^2+1}{2 \cdot 2^2}$ to $E/(j\varepsilon) = -\Lambda$ in $\Lambda = 1.5$. In Fig. 5(b), the mean-field HFB value for OP_{J^2} (49) is zero all along the path, while the exact calculation gives a very small value (note that the vertical scale is multiplied by a factor 100). In Fig. 5(c) the HFB mean-field value for $OP_{A_0^2}$ (50) jumps suddenly at $\Lambda = 1.25$ from zero to 1. The same behavior is obtained in the exact calculation. In Fig. 5(d), the HFB mean-field value for $OP_{A_1^2}$ (51) jumps suddenly from

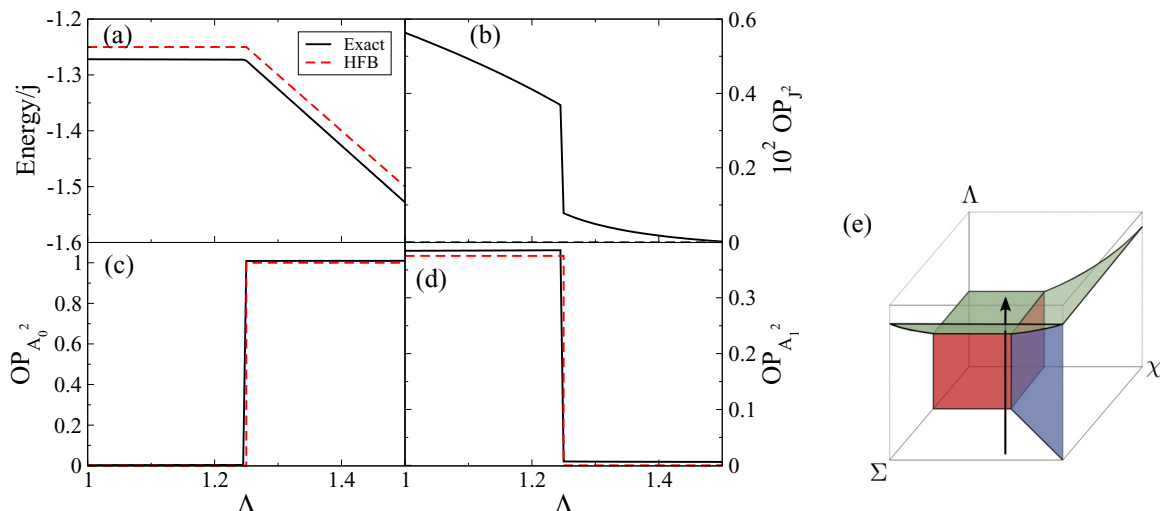


FIG. 5. Same caption as in Fig. 3 but for $\chi = 1.5$, $\Sigma = 2$, as a function of Λ . Please note that the scale in panel (b) is multiplied by 100.

$OP_{A_1^2} = \frac{2^2-1}{2 \cdot 2^2} = 0.375$ to zero at $\Lambda = 1.25$, and, once more, the exact calculation gives a consistent result. Note that this QPT involves the change from a minimum of the energy surface E_A to another one of the energy surface E_B .

All the above results confirm the structure of the phase diagram shown in Fig. 1 as well as the character, first or second order, of the QPTs.

VI. SUMMARY AND CONCLUSIONS

We have presented an extended version of the Agassi model which includes the extra $A_0^\dagger A_0$ contribution in the Hamiltonian and, therefore, it has four free parameters, ε , g , V , and h , although we have always considered a nonvanishing value for ε , and hence the number of effective free parameters is 3: $V = \frac{\varepsilon\chi}{2j-1}$, $g = \frac{\varepsilon\Sigma}{2j-1}$, and $h = \frac{\varepsilon\Lambda}{2j-1}$. We have performed a HFB mean-field approach and we have obtained the corresponding energy surfaces. It must be noted that two different energy surfaces appear, each one depending only on two of the control parameters. The existence of two different energy surfaces is due to the freedom in the election of the phase in the Bogoliubov transformation.

We have analyzed the equilibrium value of the order parameters, φ and β , for minima, maxima, and saddle points, and we have settled the phase diagram of the model. In the phase diagram four regions can be distinguished: symmetric, HF deformed, BCS deformed, and HF-BCS deformed. Moreover, there is a special situation in which the HF- and the BCS deformed minima are correlated, plane $\chi = \Sigma$. We called

this a *closed valley minimum*. In the four regions different phases can coexist; in fact, there are regions with up to three coexisting phases. In addition, there is a line in which four phases coexist and are degenerated plus a single point $\chi = \Sigma = \Lambda = 1$ in which the five phases are degenerated (spherical, HF deformed, BCS deformed, combined HF-BCS deformed, and close valley deformed minimum). The ground state is completely determined by the lowest energy minimum of the lower energy surface in each region. The existence of other minima does not affect the ground-state properties, but it is expected to have a strong influence in the presence of excited-state quantum phase transitions [19].

Finally, we have compared the exact results with the HFB mean-field values for different observables. In all the cases, good agreement has been obtained validating the mean-field results.

The phase diagram of the present extended Agassi model shows a rich variety of phases. Phase coexistence is present in extended areas of the parameter space. The model could be an important tool for benchmarking novel many-body approximations.

ACKNOWLEDGMENT

This work has been supported by the Spanish Ministerio de Economía y Competitividad and the European regional development fund (FEDER) under Projects No. FIS2014-53448-C2-1/2-P and No. FIS2015-63770-P and by Consejería de Economía, Innovación, Ciencia y Empleo de la Junta de Andalucía (Spain) under Groups FQM-160 and FQM-370.

-
- [1] F. Iachello, *Lie Algebras and Applications* (Springer-Verlag, Berlin, 2006).
 - [2] E. T. Jaynes and F. W. Cummings, Comparison of quantum and semiclassical radiation theories with application to the beam maser, *Proc. IEEE* **51**, 89 (1963).
 - [3] R. H. Dicke, Coherence in spontaneous radiation processes, *Phys. Rev.* **93**, 99 (1954).
 - [4] H. J. Lipkin, N. Meshkov, and A. J. Glick, Validity of many-body approximation methods for a solvable model. (I). Exact solutions and perturbation theory, *Nucl. Phys.* **62**, 188 (1965).
 - [5] J. Hogaasen-Feldman, A study of some approximations of the pairing force, *Nucl. Phys.* **28**, 258 (1961).
 - [6] J. P. Elliott, Collective motion in the nuclear shell model. I. Classification schemes for states of mixed configurations, *Proc. Roy. Soc. (Lond.) A* **245**, 128 (1958).
 - [7] F. Iachello and A. Arima, *The Interacting Boson Model* (Cambridge University Press, Cambridge, UK, 1987).
 - [8] P. Cejnar and J. Jolie, Quantum phase transitions in the interacting boson model, *Prog. Part. Nucl. Phys.* **62**, 210 (2009).
 - [9] P. Cejnar, J. Jolie, and R. F. Casten, Quantum phase transitions in the shapes of atomic nuclei, *Rev. Mod. Phys.* **82**, 2155 (2010).
 - [10] D. Agassi, Validity of the bcs and rpa approximations in the pairing-plus-monopole solvable model, *Nucl. Phys. A* **116**, 49 (1968).
 - [11] K. Bleuler, A. Friederich, and D. Schutte, Validity of the hartree-bogoliubov-theory in an exactly solvable model, *Nucl. Phys. A* **126**, 628 (1969).
 - [12] E. D. Davis and W. D. Heiss, Random-phase approximation and broken symmetry, *J. Phys. G: Nucl. Phys.* **12**, 805 (1986).
 - [13] Y. Gerstenmaier, Radius of convergence of the hole-line expansion and of the Rayleigh-Schrödinger perturbation series in a solvable model, *Nucl. Phys. A* **394**, 16 (1983).
 - [14] M. R. Hermes, J. Dukelsky, and G. E. Scuseria, Combining symmetry collective states with coupled cluster theory: Lessons from the Agassi model Hamiltonian, *Phys. Rev. C* **95**, 064306 (2017).
 - [15] J. G. Hirsch, P. O. Hess, and O. Civitarese, Single- and double-beta decay Fermi transitions in an exactly solvable model, *Phys. Rev. C* **56**, 199 (1997).
 - [16] J. M. Arias, J. E. García-Ramos, and J. Dukelsky, Phase Diagram of the Proton-Neutron Interacting Boson Model, *Phys. Rev. Lett.* **93**, 212501 (2004).
 - [17] J. E. García-Ramos, P. Pérez-Fernández, J. M. Arias, and E. Freire, Phase diagram of the two-fluid Lipkin model: A “butterfly” catastrophe, *Phys. Rev. C* **93**, 034336 (2016).
 - [18] L. Fortunato, C. E. Alonso, J. M. Arias, J. E. García-Ramos, and A. Vitturi, Phase diagram for a cubic-Q interacting boson model Hamiltonian: Signs of triaxiality, *Phys. Rev. C* **84**, 014326 (2011).
 - [19] J. E. García-Ramos, P. Pérez-Fernández, and J. M. Arias, Excited-state quantum phase transitions in a two-fluid Lipkin model, *Phys. Rev. C* **95**, 054326 (2017).